



Accommodation of missing shear strain in the Central Walker Lane, western North America: Constraints from dense GPS measurements



Jayne M. Bormann*, William C. Hammond, Corné Kreemer, Geoffrey Blewitt

Nevada Geodetic Laboratory, Nevada Bureau of Mines and Geology/MS 178, University of Nevada, Reno, Reno, NV 89557, USA

ARTICLE INFO

Article history:

Received 3 September 2015
Received in revised form 7 January 2016
Accepted 15 January 2016
Available online 19 February 2016
Editor: A. Yin

Keywords:

Pacific/North American plate boundary deformation
Walker Lane
geodesy
fault slip rates
transtension
comparison of geologic and geodetic slip rate data

ABSTRACT

We present 264 new interseismic GPS velocities from the Mobile Array of GPS for Nevada Transtension (MAGNET) and continuous GPS networks that measure Pacific–North American plate boundary deformation in the Central Walker Lane. Relative to a North America-fixed reference frame, northwestward velocities increase smoothly from ~ 4 mm/yr in the Basin and Range province to 12.2 mm/yr in the central Sierra Nevada resulting in a Central Walker Lane deformation budget of ~ 8 mm/yr. We use an elastic block model to estimate fault slip and block rotation rates and patterns of deformation from the GPS velocities. Right-lateral shear is distributed throughout the Central Walker Lane with strike-slip rates generally < 1.5 mm/yr predicted by the block model, but extension rates are highest near north-striking normal faults found along the Sierra Nevada frontal fault system and in a left-stepping, en-echelon series of asymmetric basins that extend from Walker Lake to Lake Tahoe. Neotectonic studies in the western Central Walker Lane find little evidence of strike-slip or oblique faulting in the asymmetric basins, prompting the suggestion that dextral deformation in this region is accommodated through clockwise block rotations. We test this hypothesis and show that a model relying solely on the combination of clockwise block rotations and normal faulting to accommodate dextral transtensional strain accumulation systematically misfits the GPS data in comparison with our preferred model. This suggests that some component of oblique or partitioned right-lateral fault slip is needed to accommodate shear in the asymmetric basins of the western Central Walker Lane. Present-day clockwise vertical axis rotation rates in the Bodie Hills, Carson Domain, and Mina Deflection are between $1\text{--}4^\circ/\text{Myr}$, lower than published paleomagnetic rotation rates, suggesting that block rotation rates have decreased since the Late to Middle Miocene.

© 2016 Elsevier B.V. All rights reserved.

1. Introduction

The Walker Lane is a ~ 100 -km-wide zone of transtensional faulting that lies between the northwest translating Sierra Nevada/Great Valley microplate and the westward extending Basin and Range province (Fig. 1) (Stewart, 1988). Up to 25% of the 50 mm/yr Pacific–North American relative right-lateral plate boundary deformation is accommodated east of the Sierra Nevada in the Walker Lane and Basin and Range (e.g. Bennett et al., 2003; Dixon et al., 2000; Thatcher et al., 1999), with the majority of the remaining motion accommodated on the San Andreas fault system (e.g. Argus and Gordon, 2001; Minster and Jordan, 1987). Deformation in the Walker Lane is considered transtensional because of

obliquity between the Sierra Nevada/Great Valley–North American microplate motion and the orientation of faults within the Walker Lane (e.g. Unruh et al., 2003; Kreemer et al., 2009) and the presence of both strike-slip and normal faulting (e.g. Stewart, 1988; Taylor and Dewey, 2009). In this study, we focus on active deformation in the Central Walker Lane, which we define as the set of normal and strike-slip faults that extend from the southern edge of the Mina Deflection north to the Carson Domain on the eastern margin of the Sierra Nevada microplate (Fig. 1).

GPS observations measure the active and ongoing contemporary deformation of the crust that is the prelude to earthquakes on faults that release a portion of the accumulated strain. The Central Walker Lane accommodates 8–10 mm/yr of right-lateral transtensional shear (Hammond and Thatcher, 2004; Oldow et al., 2001), however it remains unclear what percentage of this shear is released on mapped active fault structures and what implications the deformation has for regional seismic hazard (Wesnousky et al., 2012). Paleomagnetic and neotectonic observations identify spatially distinct zones of deformation in the Central Walker Lane

* Corresponding author. Present address: Nevada Seismological Laboratory/MS 172, University of Nevada, Reno, Reno, NV 89557, USA.

E-mail addresses: jbormann@unr.edu (J.M. Bormann), whammond@unr.edu (W.C. Hammond), kreemer@unr.edu (C. Kreemer), gblewitt@unr.edu (G. Blewitt).

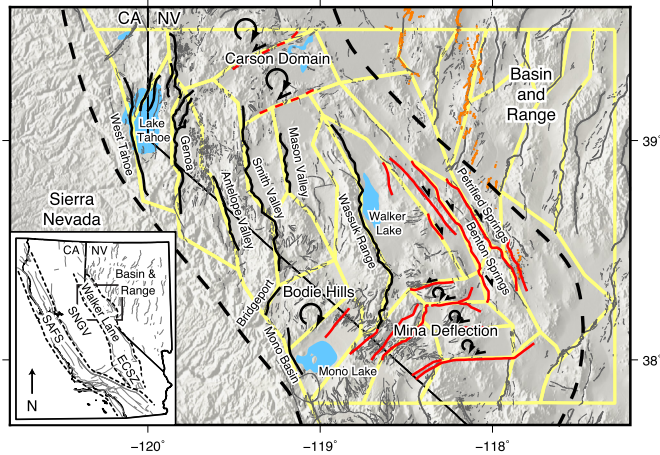


Fig. 1. Regional map showing the block model boundaries (yellow lines) in relation to the topography and faults of the Central Walker Lane. The Central Walker Lane (region within the dashed black lines) lies between the northeast striking normal faults of the Basin and Range and the Sierra Nevada microplate. Black lines delineate major normal faults of the Central Walker Lane, and red lines mark the location of strike slip faults (arrows indicate slip direction). Paleomagnetic observations indicate that crustal blocks in the Carson Domain, Bodie Hills, and Mina Deflection accommodate dextral shear through clockwise vertical axis rotations (Cashman and Fontaine, 2000; Petronis et al., 2009; Rood et al., 2011b; Carlson et al., 2013). Orange lines mark the locations of surface rupture that resulted from historic earthquakes in the Central Nevada Seismic Belt. Faults traces are modified from the USGS Quaternary Fault and Fold database (U.S. Geological Survey, California Geological Survey, Nevada Bureau of Mines and Geology, 2006). Inset map shows the location of the study area in relation to other elements of the Pacific/North America Plate boundary zone. (For interpretation of the references to color in this figure legend, the reader is referred to the web version of this article.)

with three different mechanisms of active strain release: (1) left-lateral faulting and clockwise block rotations in the Mina Deflection, Bodie Hills, and Carson Domain (e.g. Carlson et al., 2013; Cashman and Fontaine, 2000; Nagorsen-Rinke et al., 2013; Petronis et al., 2009; Rood et al., 2011b; Wesnousky, 2005a), (2) right-lateral slip on northwest trending strike slip faults in the eastern half of the Central Walker Lane (e.g. Wesnousky, 2005a), and (3) extension (e.g. Unruh et al., 2003; Wesnousky et al., 2012) and possible clockwise block rotations (Wesnousky et al., 2012) across a left-stepping series of en-echelon normal fault-bounded basins that stretch from Walker Lake to Lake Tahoe (Fig. 1). Previous geodetic studies generally conclude that transtensional deformation is distributed throughout the Central Walker Lane, however interpretations of the deformation partitioning are conflicting. Oldow (2003) and Hammond and Thatcher (2004) find a zone of shear-dominated transtension across the northwest trending strike-slip faults in the eastern Central Walker Lane and a zone of extension-dominated transtension across the normal fault-bounded basins in the western Central Walker Lane. Surplus (2008) suggests that dextral shear is concentrated only in the region that coincides with the northwest trending strike-slip faults and that deformation in the western Central Walker Lane is almost purely extensional. Unruh et al. (2003), Kreemer et al. (2009), and Hammond et al. (2011) find transtensional deformation throughout the Central Walker Lane, with a zone of both increased extension and shear along the eastern margin of the Sierra Nevada. With the exception of the Hammond et al. (2011) Northern Walker Lane study (which overlaps with our Central Walker Lane study between 38.5–39.5° latitude), none of the geodetic studies directly address how the observed transtensional strain is released through slip on active faults and block rotations.

In this study, we present a new interseismic velocity solution that combines observations from the semi-continuous Mobile Array of GPS for Nevada Transtension (MAGNET) network (Blewitt et al., 2009) with data from the EarthScope Plate Boundary Ob-

servatory (PBO) and other continuous GPS networks that measure present-day deformation in the Central Walker Lane. Our velocity solution has dense station spacing (~ 20 km) with mean velocity uncertainties of less than 0.3 mm/yr, representing a significant improvement in resolution and coverage over previously published Central Walker Lane velocity solutions (Hammond and Thatcher, 2004; Oldow et al., 2001; Oldow, 2003; Surplus, 2008). We use these velocities and the mapped traces of Central Walker Lane faults to estimate kinematically consistent fault slip and block rotation rates through an elastic block-modeling approach. Our preferred block model predicts patterns of deformation that are generally consistent with geological observations with the exception of the normal fault-bounded basins in the western portion of the Central Walker Lane. Here, the GPS data predicts oblique slip on many of the basin-bounding faults and minor clockwise rotation of the fault-bounded blocks, whereas neotectonic studies of the basin bounding faults document purely normal slip (Wesnousky et al., 2012 and references therein). We use our block model to test the hypothesis that shear deformation across these basins is accommodated through a combination of purely normal faulting and clockwise block rotations (Wesnousky et al., 2012). We demonstrate that a model that does not allow oblique slip on the basin-bounding faults systematically misfits the GPS data in comparison with our preferred model. This suggests that some component of strike-slip motion is needed to accommodate the geodetically observed shear strain in the western Central Walker Lane.

2. Central Walker Lane GPS velocities

We present horizontal velocities for 264 continuous and semi-continuous GPS stations on the Sierra Nevada/Great Valley microplate and across the Walker Lane/Basin and Range transition between 37°N–40°N and 117°W–122°W (Fig. 2 and Supplemental Table S1). Of the 264 velocities, 86 represent the motion of continuous GPS stations, and the other 178 represent the motion of semi-continuous MAGNET stations (Blewitt et al., 2009).

The GPS velocities we present in this study are calculated from daily coordinate time series derived as part of a global GPS network analysis that includes data from over 13,000 stations. We use the GIPSY-OASIS II software package (Zumberge et al., 1997) to estimate daily station position coordinates using the precise point positioning method for all GPS data available between 1996 and August 2014. The processing uses reanalyzed fiducial-free GPS satellite orbit and clock parameters provided by the Jet Propulsion Laboratory's IGS Analysis Center with antenna calibration models for station receivers and satellite transmitters. The observation model includes solid earth tides and oceanic tidal loading (Scherneck, 1991). The Global Mapping Function was applied to model tropospheric refractivity (Boehm et al., 2006), and the tropospheric wet delay was modeled as a random walk zenith parameter with two random walk horizontal gradient parameters (Bar Sever et al., 1998). The carrier phase ambiguities are resolved using the WLPB method (Bertiger et al., 2010).

We align the daily position solutions with a custom North America-fixed, spatially filtered reference frame, NA12 (Blewitt et al., 2013). NA12 has an origin and scale that is consistent with the International Terrestrial Reference Frame, ITRF2008. The seven-parameter daily coordinate transformations from the JPL fiducial-free frame to NA12 are publicly available for GIPSY-OASIS II users at [ftp://gneiss.nbmj.unr.edu/x-files](http://gneiss.nbmj.unr.edu/x-files), and the daily position time series data are available and plotted at <http://geodesy.unr.edu>. We correct the daily coordinate time series to remove the effects of transient deformation resulting from postseismic viscoelastic relaxation following historic surface rupturing earthquakes in the Central Nevada Seismic Belt (Gourmelen and Amelung, 2005; Hammond et al., 2009) using the method of Hammond et al. (2010)

and the preferred western Basin and Range viscosity model determined by Hammond et al. (2009). For stations that have more than 2.5 years of data, we estimate velocities from both the original and postseismic relaxation corrected time series accounting for annual and semiannual periodic seasonal deformation and step function offsets that correspond to known equipment changes (Supplemental Table S1).

The velocity uncertainties were estimated using the Hector software package (Bos et al., 2013), which uses the Maximum Likelihood Estimation method to estimate rates while estimating contributions from white plus power law noise. For the postseismic corrected rates, we also include uncertainty associated with the viscoelastic model of the lower crust and upper mantle used in the correction. To determine this uncertainty, we estimate the variance in velocities predicted by the set of viscoelastic models determined by Hammond et al. (2009) to fit the GPS and InSAR measured deformation in Central Nevada (after Hammond et al., 2011). We combine the Hector uncertainties with the postseismic viscoelastic relaxation model correction uncertainties using the square root of the sum of squares. As uncertainties associated with time correlated noise decrease with increased time-series length and the uncertainty in the postseismic correction decreases with distance from the CNSB, uncertainties estimated in this manner may be too small for long-running stations that are far from the CNSB earthquakes. We apply an uncertainty floor of 0.15 mm/yr in both the east and north directions, consistent with the inferred horizontal accuracy of the longest-running stations in stable North America (Blewitt et al., 2013). This value is low enough to give the continuous stations significantly greater weight than the MAGNET velocities in the inversion, but not so low that uncertainties are unrealistic and cause the MAGNET velocities to be ignored.

We exclude from our analysis stations that have (1) horizontal velocity uncertainties greater than 2 mm/yr, or (2) visually outlying velocities or vertical velocities greater than 5 mm/yr, as these measurements may be influenced by anthropogenic or other non-tectonic geologic processes. Additionally, we omit the velocities of MAGNET sites RENO, MOGL, and VRDE because the time series include coseismic offsets and afterslip resulting from the 2008 Mogul seismic swarm in west Reno (Blewitt et al., 2008) and GPS sites near the Long Valley caldera because the stations record motion resulting from inflation and deflation in response to magmatic movements within the caldera (e.g. Marshall et al., 1997; Newman et al., 2001; Langbein, 2003).

The primary feature of the velocity field is a smooth and continuous east-to-west increase in the northwestward velocity from GPS sites in the Basin and Range to sites on the Sierra Nevada/Great Valley microplate (Fig. 2, upper panel). The smoothness of our velocity solution is in contrast with the apparent complexity of previous campaign-based velocity solutions (Oldow et al., 2001; Oldow, 2003). The interseismic velocities corrected for postseismic relaxation increase from ~ 4 mm/yr in the Basin and Range to 12.2 mm/yr at sites P245 and P308 in the central part of the Sierra Nevada/Great Valley microplate (Fig. 2, lower panel). Our Central Walker Lane velocity increase of 8 mm/yr is slightly less than the 10 mm/yr of differential motion reported by Oldow et al. (2001), with the 2 mm/yr reduction in relative motion resulting largely from the postseismic relaxation correction. The similarity between the two relative motion budgets is a testament to the value of campaign-style GPS observations in resolving broad patterns of deformation, even in relatively slowly deforming regions.

Despite geographic segmentation in the style and orientation of faults within the Central Walker Lane, we do not find clear visual evidence of distinct deformational domains in the GPS velocities (Figs. 2 and 3A, left panel). The distance between the 5–11 mm/yr contours gradually widens from south to north, how-

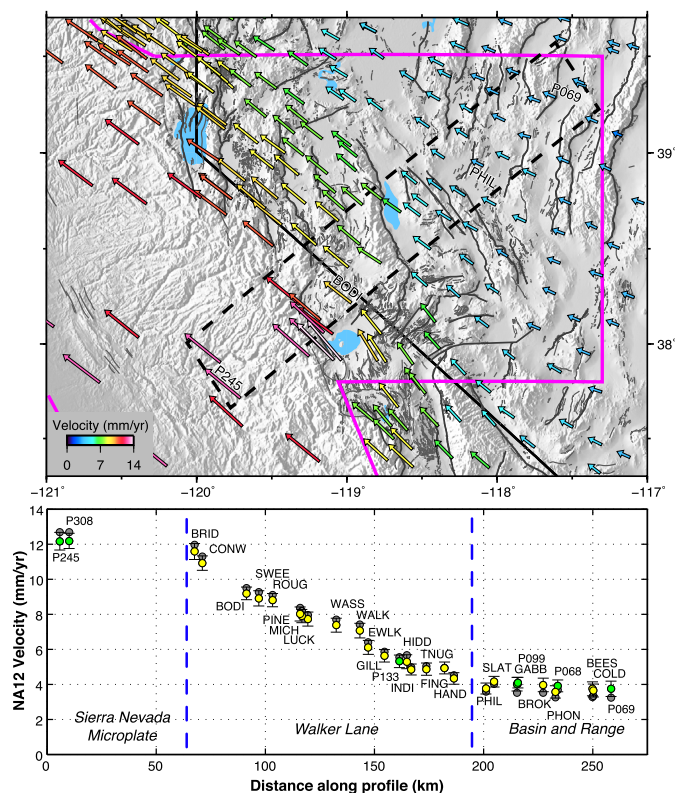


Fig. 2. Interseismic GPS velocities in the NA12 North America reference frame. (Top) GPS velocities across the Basin and Range, Central Walker Lane, and Sierra Nevada transition. Velocity magnitude is indicated by the length and color of the arrows. Dashed box marks the location of the velocity profile shown below. Selected GPS sites within the profile are labeled with the site names. (Bottom) Magnitude of the GPS velocity for a 50-km-wide transect of sites that is perpendicular to the trend of the Central Walker Lane. Gray circles are the observed rates, and the yellow (MAGNET stations) and green (continuous stations) circles with 2 sigma error bars are the interseismic rates corrected for the effects of viscoelastic postseismic relaxation following historic earthquakes in the Central Nevada Seismic Belt (Hammond et al., 2009). Blue dashed lines indicate east and west bounds of Walker Lane. (For interpretation of the references to color in this figure legend, the reader is referred to the web version of this article.)

ever the 5–7 mm/yr contours pass directly through the Mina Deflection without any offset corresponding to right step in faulting from the Southern Walker Lane to the Central Walker Lane. Decomposing the velocities into the north and west components highlights two interesting features that are not distinguishable when we consider only the total rates: (1) a zone of increased northward velocities in the Mono Lake basin (Fig. 3A, center panel, 38°N and 119°W) and (2) a constriction of the 5–8 mm/yr westward velocity contours to the south of the Mina Deflection and a pronounced eastward step in the 5–6 mm/yr contours north of the Mina Deflection (Fig. 3A, right panel).

When the Central Walker Lane GPS velocities are viewed in a reference frame with a fixed Sierra Nevada/Great Valley microplate, small gradients in velocity near the Sierra Nevada/Walker Lane transition are emphasized and more easily interpreted. In order to view velocities with respect to the Sierra Nevada, we must first solve for the rigid-body motion of the block. We use 33 velocities distributed along the length of the Sierra Nevada/Great Valley microplate to calculate a rotation rate of $0.1^{\circ}/\text{Myr}$ around a pole located at -32.6° latitude and -116.3° longitude (Block 1, Supplemental Table S2). We subtract the predicted rotation from our NA12 velocities to obtain velocities with respect to a fixed Sierra Nevada block (Fig. 4). GPS stations east of the Sierra Nevada crest typically move southeast, consistent with deformation associated with Pacific–North American relative plate motion. However, in the

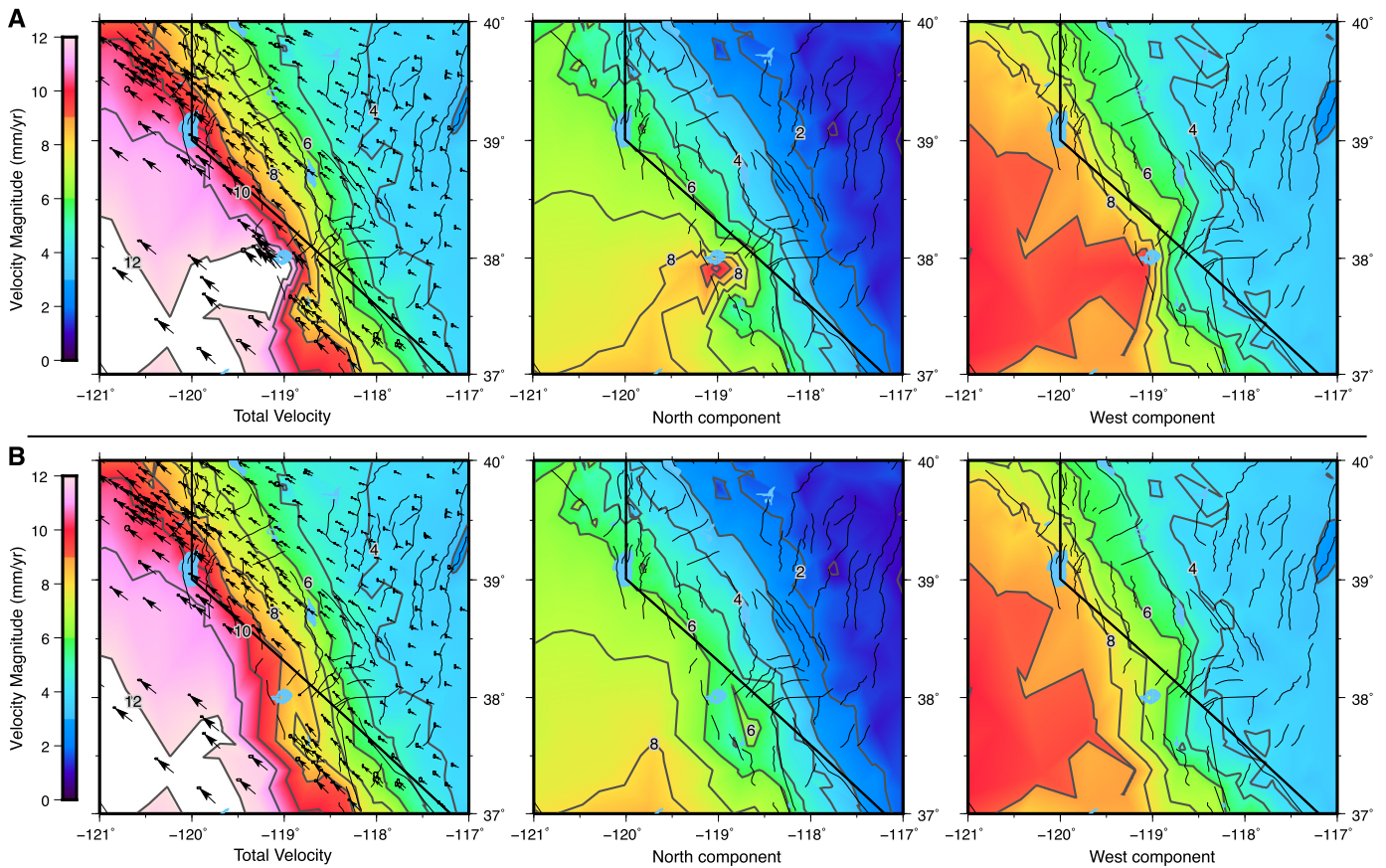


Fig. 3. Plots showing contours of the total GPS velocities (left panel) and the north and west velocity components (center and right panels). (A) Plots include the anomalous Mono Basin velocities, and (B) plots without the Mono Basin velocities. (For interpretation of the colors in this figure, the reader is referred to the web version of this article.)

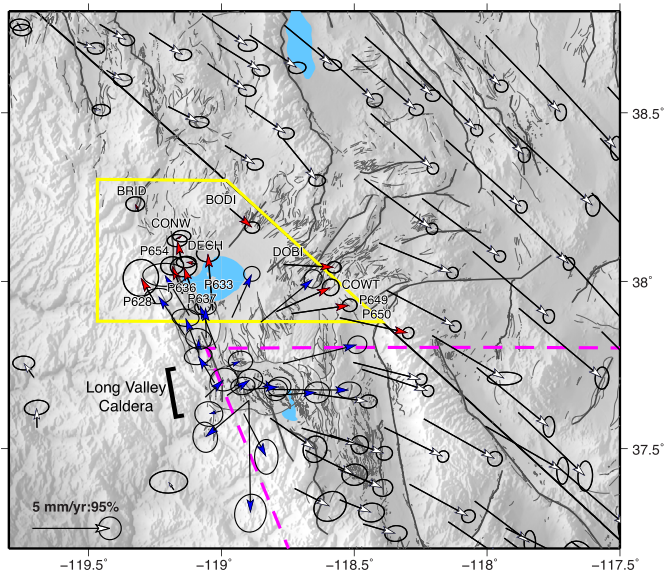


Fig. 4. CWL GPS velocities with respect to the motion of the Sierra Nevada block. The yellow box outlines velocities in the vicinity of the Mono Basin that are deflected to the north and east (red vectors). Blue vectors represent the motion of GPS stations that are affected by magmatic activity in the Long Valley Caldera. The dashed magenta line marks the extent of the block model area. White GPS velocities to the north and west of this boundary are used in the block modeling analysis. (For interpretation of the references to color in this figure legend, the reader is referred to the web version of this article.)

vicinity of the Mono Lake basin, 13 GPS stations move to the north and east, in the opposite direction expected to result from plate boundary deformation. Because of the Mono Basin's close prox-

imity to the Long Valley Caldera, the history of young volcanism in the Mono-Inyo Craters (Sieh and Bursik, 1986), and possible present-day episodes of dike injection along the chain of craters (Marshall et al., 1997; Feng and Newman, 2009), we exclude these GPS stations from the subset of the velocity solution used for the block model analysis as their motion is likely influenced by transient magmatic activity.

The pattern of the westward velocity contours near the Mina deflection (Fig. 3A, right panel) suggests that extension along the central Sierra Nevada frontal fault system is highest in the Southern Walker Lane and immediately to the west of the Mina Deflection in the Mono Lake Basin, but that extension is more evenly distributed along the normal fault bounded basins in the Central Walker Lane. However, this interpretation is uncertain as we demonstrated that GPS velocities in the Mono Lake Basin are deflected anomalously to the north and east. Omitting the Mono Basin velocities leaves the distribution of the westward velocity contours across the normal fault-bounded basins unchanged, but extension along the Sierra Nevada range front in the Southern Walker Lane and Mono Lake Basin is considerably less focused, as there is no data available to constrain the contours (Fig. 3B, right panel).

3. Block model methodology and results

We use the GPS velocity solution and an elastic block model to constrain kinematically consistent fault slip and block rotation rates for the Central Walker Lane between 37.8° to 39.5° latitude and 117.3° longitude west to the Sierra Nevada at approximately 120.5° longitude. Block modeling techniques implement the “back slip” method of Savage (1983) to describe the interseis-

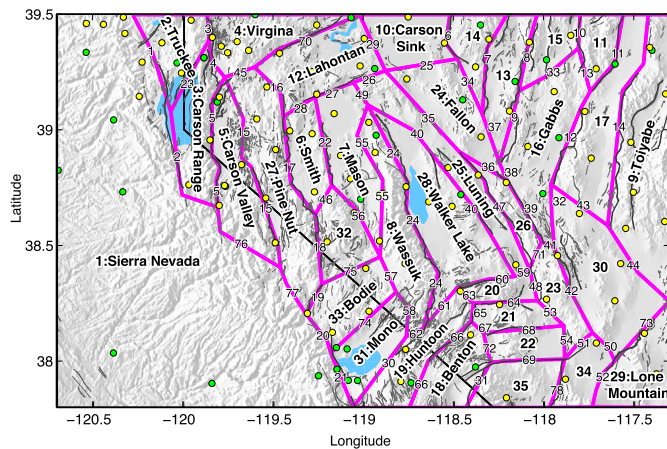


Fig. 5. Block boundaries used for the deformation analysis with block name and fault train legend. Magenta lines illustrate block model geometry with faults, topography, and GPS station locations. Yellow circles represent MAGNET stations, and green circles represent continuous stations. Bold numbers and names identify the location of blocks referred to in the text and in Table S2. Smaller numbers identify fault trains whose slip rates are reported in Table S3. (For interpretation of the references to color in this figure legend, the reader is referred to the web version of this article.)

mic GPS velocity field as the sum of the long-term block motion minus the local and temporary effects of elastic strain accumulation on the locked block-bounding faults (e.g. Bennett et al., 1996; McCaffrey, 2002; Meade and Hager, 2005).

Faulting in the Central Walker Lane is discontinuous and complex in comparison with the structurally mature faults in the San Andreas system (Wesnousky, 2005b). Accurately representing this geologic complexity guides the development of our block model geometry and is essential to produce our best estimate of block rotation and fault slip rates. We draw block boundaries first to coincide with the surface traces of major active faults (modified from fault sources in the 2008 National Seismic Hazard Maps, Petersen et al., 2008, and the USGS Quaternary Fault and Fold database, USGS, CGS, and NBMG, 2006) and we connect these segments following the traces of minor faults, patterns of seismicity, and major topographic features (Fig. 1 and Fig. 5). Our model divides the Central Walker Lane into 35 blocks separated by 78 fault trains, and it represents a simplification of known Quaternary active faults. Further simplification of the model geometry would require the assumption that a mapped active fault is not slipping, thereby violating geologic observations of fault slip.

We use the motion of the 142 GPS stations located within the block model boundaries (Table S1 in the supplemental material) to solve simultaneously for the long-term motion of each block and the dip-slip and strike-slip components of fault slip rate through a regularized weighted least squares inversion using the methodology of Hammond et al. (2011). This methodology enforces kinematic consistency by imposing a strict regularization constraint that requires consistency between relative block motions and fault slip rates, the α parameter. The method also includes two stochastic damping parameters that minimize fault slip rates and block centroid vertical axis rotations or spin rates, the γ and β parameters. We assign fault dip and locking depth, and our method allows us to constrain slip rates or block rotations to match specific values (e.g., published geologic slip rate or plate rotation estimates). Optimal values of the regularization parameters result in smooth and simple models that fit the GPS data well. We use identical values to Hammond et al. (2011), with the exception of the β parameter, which we increase by a factor of ~ 3 to allow blocks in the Mina Deflection and Carson Domain to spin on vertical axes more freely (Table 1).

Table 1
Model assumptions and regularization parameters.

Type	Value
Strike-slip fault dip	80°
Normal fault dip	45°
Locking depth (L)	15 km
Poisson's ratio (ν)	0.25
Shear modulus (μ)	3×10^{10} Pa s
Slip rate consistency (α)	10^{-6} m/yr
Block centroid vertical axis rotation damping (β)	10×10^{-9} rad/yr
Slip rate damping (γ)	4×10^{-4} m/yr

We constrain the motion of the Sierra Nevada block to match our calculated Sierra Nevada/Great Valley rotation rate (Block 1, Supplemental Table S2) and solve for the block's uniform horizontal tensor strain rate from the rotation model residuals. Deformation within the Sierra Nevada/Great Valley microplate is primarily shear strain, with the block extending at a rate of 5.9 ± 1.0 nanostrain/yr in the N71°E direction and contracting at a rate of 6.5 ± 0.6 nanostrain/yr in the N19°W direction. Although these strain rates are low, they are important to account for due to the long and narrow shape of the block. For example, contractional deformation sub-parallel to the long axis of the Sierra Nevada introduces velocity gradients of >2 mm/yr in the N19°W direction over the ~ 550 km length of the block. We impose strain within the Sierra Nevada block at two-thirds of our calculated rate, and we strictly enforce our rotation and strain constraints for the Sierra Nevada block to ensure a stable western boundary condition when testing different hypotheses with our block model.

The resulting block model predicts partitioned zones of (1) right-lateral slip and northwest translation of blocks along northwest striking faults in the eastern Central Walker Lane, (2) left-lateral slip and clockwise block rotations in regions of east and northeast striking faults in the Bodie Hills, Mina Deflection and Carson Domain, and (3) right-lateral oblique normal slip on north striking faults along the Sierra Nevada frontal fault system and between the Walker Lake–Lake Tahoe basins (Fig. 6A and B). The model residuals are small and randomly oriented (Fig. 6C), with residual root mean square (RMS) misfits in the east (north) velocities of 0.43 (0.40) mm/yr. The block rotation and fault slip rates are provided in Tables S2 and S3 in the supplemental material. The highest rates of right-lateral slip are predicted along the Sierra Nevada frontal fault in the Mono Lake Basin and on the northward continuation of that structure in Antelope Valley (Fig. 1; fault trains 20, 21, 77 and 15 respectively, Fig. 5 and Table S3). Lower, but significant rates of right-lateral slip are predicted on the Wassuk Range fault zone and on the Benton Springs fault (Fig. 1; fault trains 24 and 35, 47 respectively, Fig. 5 and Table S3). Blocks in the Carson Domain and Mina Deflection rotate the fastest, with clockwise spin rates between 2.0–2.5°/Myr (Fig. 1; blocks 4, 12 and 18, 19, 21, 22, 35 respectively, Fig. 5 and Table S2), with slightly slower clockwise rotation rates of 1.1–1.3 °/Myr in the Bodie Hills (Fig. 1; blocks 31 and 33, Fig. 5 and Table S2).

4. Discussion

The patterns of deformation predicted by the block model are largely consistent with geologic observations with the exception of the right-lateral oblique normal slip along the Sierra Nevada frontal fault system and the Walker Lake to Lake Tahoe basin-bounding, north striking faults and localized regions of minor predicted compression across normal fault block boundaries on the Sierra Nevada block. Wesnousky et al. (2012) explored the discrepancy between geologic observations and the deformation implied by the GPS velocity field in these normal fault-bounded basins. They concluded that shear deformation in this part of the Walker

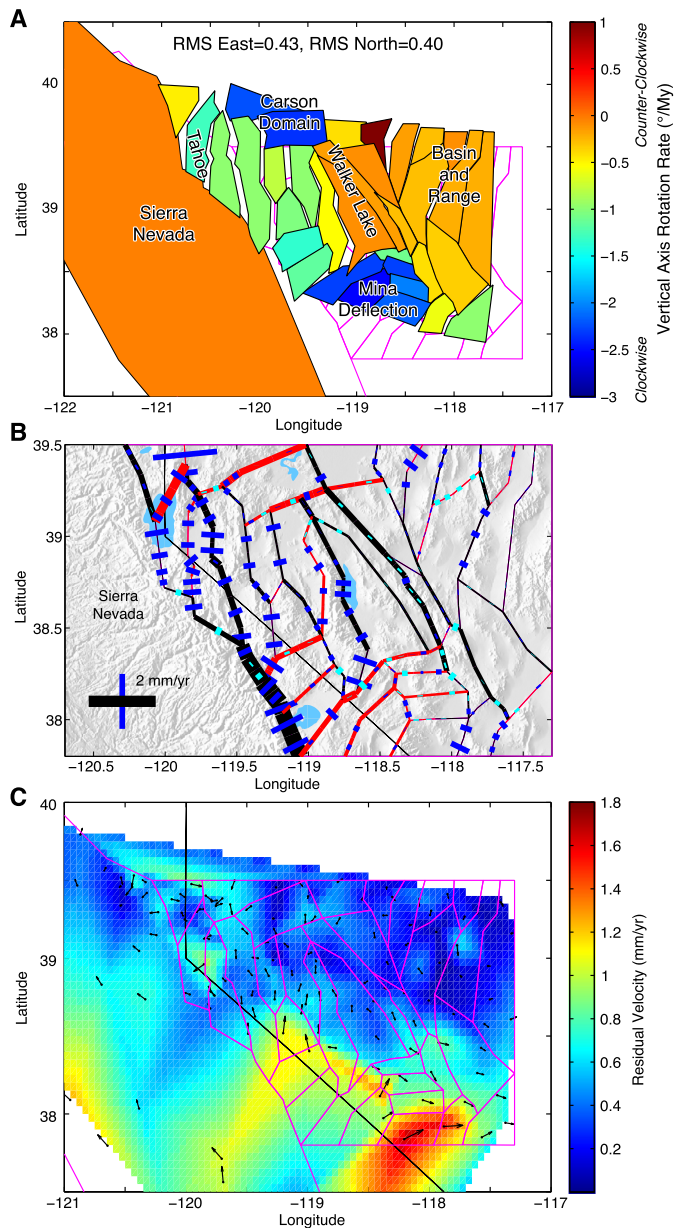


Fig. 6. Block motions, slip rates, and velocity residuals for the best fitting GPS model. (A) Rigid block rotation and translation (Supplemental Table S2) exaggerated by a factor of 10^7 (representing 10 million years of deformation). Color of block indicates vertical axis rotation rate. (B) Predicted fault slip rates (Supplemental Table S2) represented by the thickness of black (red) line for dextral (sinistral) strike-slip motion and the length of blue (cyan) bar for fault normal extension (compression). (C) Residual GPS velocities (black arrows) after subtracting the model predictions. The colored surface represents an interpolation of the residual magnitude, with warm colors indicating the regions of greatest misfit. (For interpretation of the references to color in this figure legend, the reader is referred to the web version of this article.)

Lane is likely accommodated through a combination of normal faulting and clockwise vertical axis block rotations. We test this hypothesis in a block model where we constrain slip on the Sierra Nevada frontal fault and north trending basin-bounding faults to be purely dip-slip by assigning the strike-slip component of the slip rates to be zero (Fig. 7). This model predicts increased clockwise block rotation rates throughout the Central Walker Lane and reproduces the asymmetric basin shape documented by Wesnousky et al. (2012) (Fig. 7A) supporting the mechanism of shear accommodation through normal faulting and clockwise block rotations. However, this model systematically misfits the GPS data with

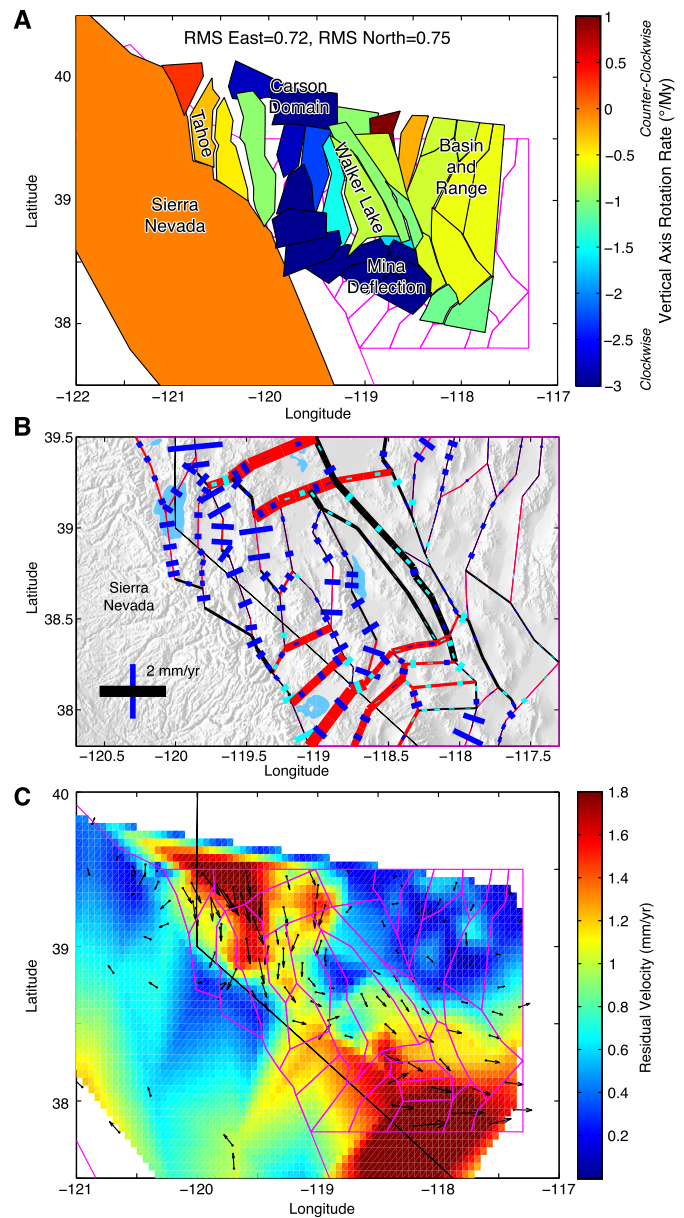


Fig. 7. Same as Fig. 6, except that the model is constrained to be consistent with the geologic observations that preclude oblique dextral/normal slip on Central Walker Lane normal faults (Fig. 1). (For interpretation of the colors in this figure, the reader is referred to the web version of this article.)

southward velocity residuals as large as 1.5–2.0 mm/yr in the western Central Walker Lane (Fig. 7C). Our preferred model is more consistent with the GPS data (Fig. 6C), which suggests that a component of oblique slip is needed on or near the Sierra Nevada frontal fault zone and other north trending, basin-bounding faults to fully accommodate the geodetically observed dextral shear.

Although clockwise block rotations alone cannot accommodate all of the geodetically observed right-lateral strain in the absence of optimally oriented strike-slip faults, paleomagnetic studies indicate that block rotations do play a significant role in regional strain accommodation (Carlson et al., 2013; Cashman and Fontaine, 2000; Rood et al., 2011b). The two block models presented here provide end-member constraints on present-day block rotations rates in the Central Walker Lane. Our preferred model (Fig. 6), that is constrained only by the GPS data, predicts clockwise block rotation rates of 2.2–2.3°/Myr in the Carson Domain and 2.0–2.5°/Myr in the Mina Deflection, with lower clockwise rotation rates between

Table 2

Geologic and geodetic estimates of fault slip rates for the en-echelon, normal fault-bounded basins.

Fault ^a	Basin	Block model fault train ^b	Geologic horizontal extension rate (mm/yr) ^c	GPS fault perpendicular extension (mm/yr) ^d	GPS fault parallel shear (mm/yr) ^{d,e}	Block model horizontal extension rate (mm/yr)	Block model strike-slip rate (mm/yr) ^e
West Tahoe		2				0.5 ± 0.4	0.2 ± 0.4
Stateline	Tahoe	23	0.5–1.7	0.6–0.8	0.5–0.7	0.6 ± 0.5	1.6 ± 0.5
Incline Village							
Genoa Central	Carson	5	0.7–1.7	1.0–1.3	~0.1	0.6 ± 0.5	0.2 ± 0.5
Genoa South	Carson		0.1–0.5	0.6–0.9	~0.3		
Smith Valley	Smith	17	0.1–0.3	0.7–1.2	1.0–1.2	0.4 ± 0.5	0.5 ± 0.4
Singatse Range	Mason	22	0.2–0.3	0.7–0.9	0.1 –0.2	0.6 ± 0.5	0.4 ± 0.4
Antelope Valley	Antelope	15	0.35	0.9–1.1	0.6–1.1	0.7 ± 0.5	1.1 ± 0.4
Robinson Creek	Bridgeport	19	0.1–0.3	~0.2	0.0–0.1	1.2 ± 0.5	1.3 ± 0.6
Wassuk Central	Walker Central		0.5–0.8	0.4–0.7	1.2–1.6		
Wassuk North ^{f,g}	Walker North	24	0.5–1.3	0.9–1.0	0.7–1.3	0.6 ± 0.4	0.7 ± 0.3

^a Geologic fault slip rates from [Wesnousky et al. \(2012\)](#) and references therein, with the exception of recently published rates for the northern Wassuk Range fault zone.

^b See [Fig. 5](#) for fault train legend.

^c Rates calculated in [Wesnousky et al. \(2012\)](#) and this study (Wassuk North site) from originally reported vertical and dip-slip rates by assuming a fault dip of 45–60°.

^d Rates calculated by [Wesnousky et al. \(2012\)](#).

^e Bold slip rates indicate left-lateral motion.

^f [Dong et al. \(2014\)](#).

^g [Surpless and Kroeger \(2015\)](#).

1.1–1.3°/Myr in the Bodie Hills and 0.5–1.2°/Myr in the en-echelon normal fault-bounded basins ([Fig. 1](#); blocks 3, 5, 6, 7, 8, and 27, [Fig. 5](#) and Table S2). In general, our rotation rates for blocks in the Carson Domain and region of normal fault-bounded basins are approximately twice the rates predicted for the same regions in the [Hammond et al. \(2011\)](#) Northern Walker Lane block model. The increased rotation rates are largely due to our decision to relax the β regularization parameter, which minimizes block centroid vertical axis rotations, to allow blocks to rotate more freely. Differences in block geometry parameterization also contribute to our increased rotation rates in the Carson Domain. The [Hammond et al. \(2011\)](#) model divides our rectangular-shaped Lahontan block (block 12, [Fig. 5](#)), which is defined by the Carson Lineament to the north and the Wabuska Lineament to the south, into two smaller blocks separated by a northwest-striking fault ([Hammond et al., 2011](#), Fig. 8, blocks 24 and 29). The presence of a northwest-striking fault allows the blocks to translate right-laterally, whereas in our model, the Lahontan block must rotate to accommodate the northwest velocities that increase to the west.

When we constrain the block model to only allow dip-slip motion on the Sierra Nevada frontal fault and the normal fault bounded basins ([Fig. 7](#)), the clockwise block rotation rates increase to 2.8–3.3°/Myr in the Carson Domain, 3.0–4.1°/Myr in the Mina Deflection, 3.5–3.8°/Myr in the Bodie Hills, and 1.4–2.8°/Myr in the Smith Valley, Mason Valley, and Wassuk Range blocks of the en-echelon basins ([Fig. 1](#) and [Fig. 5](#), giving us maximum limits on the present-day rotation rates. The rotation rates from our preferred model are slightly lower than published paleomagnetic vertical axis rotation rates in the Central Walker Lane of 3–6°/Myr inferred from 37–51° of clockwise rotation in 9–13 Ma basalts in the Carson Domain ([Cashman and Fontaine, 2000](#)), and 5 ± 2°/Myr since the Middle Miocene in the Bodie Hills ([Rood et al., 2011b](#)). The lower present-day rotation rates predicted by our preferred model may be interpreted to suggest that block rotation rates have decreased over time as rates of faulting increase due to structural maturation of the Walker Lane (e.g. [Carlson et al., 2013](#); [Hammond et al., 2011](#)), however the maximum constraints from the dip-slip only model are compatible with the lower end of the paleomagnetic estimates.

Because kinematic consistency requires that block models account for the component of the GPS velocity field attributable to long-term block translations and rotations when estimating fault slip rates, the horizontal extension and strike-slip rates predicted by our preferred model are generally lower than the deformation

rates reported in [Wesnousky et al. \(2012\)](#) ([Table 2](#)). Although the GPS velocity field is smooth, right-lateral slip is not evenly distributed throughout the en-echelon fault-bounded basins in the block model. Rather, the block model predicts that right-lateral slip is predominantly accommodated on the Sierra Nevada frontal fault in the Mono Lake Basin and the northward continuation of this structure in Antelope Valley and along the Wassuk Range fault zone. The other north-striking faults each accommodate less than 0.5 mm/yr of right-lateral slip.

The uneven distribution of right-lateral slip throughout the normal fault-bounded basins suggests that the accommodation of Walker Lane shear may not be explained by a single regional scale mechanism, but rather through a combination of different mechanisms. Alternative mechanisms to accommodate right-lateral shear include oblique slip on the basin bounding faults or partitioned slip where shear is accommodated on strike-slip faults outboard of the range front faults. These mechanisms are supported by suggestions of right-lateral offset reported along both the Antelope Valley and Wassuk Range basin-bounding range front faults ([Wesnousky, 2005a](#); [Sarmiento et al., 2011](#)), and by the discovery of a right-lateral strike-slip fault with a slip rate of ~1 mm/yr outboard of the Wassuk range front normal fault ([Dong et al., 2014](#)). Although neotectonic evidence for right-lateral shear is sparse, it is possible that lateral offset is poorly recorded on these slowly moving faults due to erosional landform degradation over the longer time interval needed to accumulate appreciable offset (e.g. [Gold et al., 2013](#)), or that the dextral deformation is diffuse, with right-lateral slip distributed across many small faults rather than occurring on a single integrated fault structure. Focal mechanisms and moment tensor solutions for moderately sized historical earthquakes in the Central Walker Lane record both strike-slip and normal events (e.g. [Ichinose et al., 2003](#)). These observations are consistent with the style of geodetically observed Central Walker Lane transtensional deformation, however most of the historical earthquakes occur off of major active faults structures or in the stepovers between fault systems, giving no straightforward insight into the style of deformation on Sierra Nevada frontal fault system and on basin-bounding normal faults.

Explaining the high rates of both strike-slip and horizontal extension along the Sierra Nevada frontal fault near the Mono Lake Basin is not straightforward. There are no geologic suggestions of right-lateral slip along this section of frontal fault system, however the high slip rates correspond to the location of the tightest north and west GPS velocity contours in the Central Walker Lane ([Fig. 3](#))

and the highest rates of extension along the Sierra Nevada frontal fault system (Rood et al., 2011a). Here, the high right-lateral slip and horizontal extension rates in the model may be partially accommodated through dike injections along the Mono-Inyo Craters (Riley et al., 2012) or by higher vertical axis rotation rates in the Bodie Hills and Mina Deflection (Carlson et al., 2013; Rood et al., 2011a, 2011b).

5. Conclusions

The velocity field we present in this study represents a significant improvement in resolution over previously published Central Walker Lane GPS velocities. We combine spatially dense semi-continuous GPS observations from MAGNET with continuous GPS observations from the EarthScope Plate Boundary Observatory to show that GPS velocities in the northwest direction increase smoothly by 8 mm/yr across the Central Walker Lane. We use this velocity data to constrain fault slip and block rotation rates in the Central Walker Lane through an elastic block modeling approach. The patterns of deformation predicted by the block model are generally in agreement with neotectonic observations of active faulting, however our model differs from geologic observations by predicting right-lateral slip rates between 0.2–1.1 mm/yr in addition to extension on north-striking faults between and including the Walker Lake and Lake Tahoe basins. Although clockwise vertical axis block rotations do accommodate some of the right-lateral shear in the Carson Domain, Mina Deflection, and across the normal fault-bounded basins, we show that it is not possible to fit the GPS observations with models that do not allow right-lateral oblique extension on the Sierra Nevada frontal fault and the en-echelon series of basins between Walker Lake and Lake Tahoe. The slip rates predicted by our kinematically consistent block model are generally lower than deformation rates inferred directly from GPS velocity gradients (Wesnousky et al., 2012), highlighting the importance of accounting for block rotations when estimating fault slip rates from GPS data for seismic hazard studies. The models we present constrain present-day clockwise rotation rates to be between 1.2°–3.9°/Myr in the Carson Domain, Mina Deflection, and Bodie Hills and between 1.0°–2.6°/Myr across the en-echelon, normal fault bounded basins in the western half of the Central Walker Lane.

Acknowledgements

We thank Brendan Meade, Wayne Thatcher, and an anonymous reviewer for constructive comments that improved this manuscript. Funding for this work was primarily provided by NSF grant EAR-0635757 as part of the EarthScope program. Additional data collection was funded by a graduate student research grant from the Geological Society of America. Support for GPS surveys, network and modeling development was provided by the NSF Tectonics and EarthScope programs under EAR projects 0844389, 0610031, and 1252210. The USGS Geodetic Network Support Program supplied additional support for GPS surveying (Award Nos. G10AC00138 and G15AC00078). We thank UNAVCO, Inc., for operation and maintenance of the EarthScope Plate Boundary Observatory and archiving of the GPS data used in this study, and the Jet Propulsion Laboratory for use of the GIPSY-OASIS II software and for providing GPS products. Special thanks go to Bret Pecoraro for providing essential MAGNET field support. Hans-Peter Plag, Sumant Jha, Xiaohui Zhou, Jay Goldfarb, and Yang Zhang also provided assistance with GPS data collection. Figs. 1–5 were generated all or in part by the Generic Mapping Tools software of Wessel et al. (2013).

Appendix A. Supplementary material

Supplementary material related to this article can be found online at <http://dx.doi.org/10.1016/j.epsl.2016.01.015>.

References

- Argus, D., Gordon, R., 2001. Present tectonic motion across the Coast Ranges and San Andreas fault system in central California. *Geol. Soc. Am. Bull.* 113 (12), 1580–1592.
- Bar Sever, Y.E., Kroger, P.M., Borjesson, J.A., 1998. Estimating horizontal gradients of tropospheric path delay with a single GPS receiver. *J. Geophys. Res.* 103, 5019–5035. <http://dx.doi.org/10.1029/97JB03534>.
- Bennett, R.A., Wernicke, B.P., Niemi, N.A., Friedrich, A.M., Davis, J.L., 2003. Contemporary strain rates in the northern Basin and Range province from GPS data. *Tectonics* 22 (2), 1008. <http://dx.doi.org/10.1029/2001TC001355>.
- Bennett, R.A., Rodi, W., Reilinger, R.E., 1996. Global Positioning System constraints on fault slip rates in southern California and northern Baja, Mexico. *J. Geophys. Res.* 101 (B10), 21943–21960. <http://dx.doi.org/10.1029/96JB02488>.
- Bertiger, W., Desai, S.D., Haines, B., Harvey, N., Moore, A.W., Owen, S., Weiss, J.P., 2010. Single receiver phase ambiguity resolution with GPS data. *J. Geod.* 84, 327–337. <http://dx.doi.org/10.1007/s00190-010-0371-9>.
- Blewitt, G., Kreemer, C., Hammond, W.C., Goldfarb, J., 2013. Terrestrial reference frame NA12 for crustal deformation studies in North America. *J. Geodyn.* 72, 11–24. <http://dx.doi.org/10.1016/j.jog.2013.08.004>.
- Blewitt, G., Bell, J.W., Hammond, W.C., Kreemer, C., Plag, H.-P., dePolo, C.M., 2008. GPS and InSAR monitoring of the Mogul Swarm: evidence for mainly aseismic fault creep, with implications for seismic hazard. *Eos Trans. AGU* 89 (53), Fall Meet. Suppl., Abstract S53C-03.
- Blewitt, G., Hammond, W.C., Kreemer, C., 2009. Geodetic observation of contemporary deformation in the Northern Walker Lane: 1. Semipermanent GPS strategy. In: Oldow, J.S., Cashman, P.H. (Eds.), *Late Cenozoic Structure and Evolution of the Great Basin–Sierra Nevada Transition*. In: *Spec. Pap., Geol. Soc. Am.*, vol. 447, pp. 1–15.
- Boehm, J., Niell, A., Tregoning, P., Schuh, H., 2006. Global mapping function (GMF): a new empirical mapping function based on numerical weather model data. *Geophys. Res. Lett.* 33, L07304. <http://dx.doi.org/10.1029/2005GL025546>.
- Bos, M.S., Fernandes, R.M.S., Williams, S.D.P., Bastos, L., 2013. Fast error analysis of continuous GNSS observations with missing data. *J. Geod.* 87, 351–360. <http://dx.doi.org/10.1007/s00190-012-0605-0>.
- Carlson, C.W., Pluhar, C.J., Glen, J.M.G., Farner, M.J., 2013. Kinematics of the west-central Walker Lane: spatially and temporally variable rotations evident in the Late Miocene Stanislaus Group. *Geosphere* 9 (6), 1520–1551. <http://dx.doi.org/10.1130/GES00955.1>.
- Cashman, P., Fontaine, S.A., 2000. Strain partitioning in the northern Walker Lane, western Nevada and northeastern California. *Tectonophysics* 326 (1–2), 111–130.
- Dixon, T.H., Miller, M., Farina, F., Wang, H., Johnson, D., 2000. Present-day motion of the Sierra Nevada block and some tectonic implications for the Basin and Range province, North American Cordillera. *Tectonics* 19, 1–24. <http://dx.doi.org/10.1029/1998TC001088>.
- Dong, S., Gulsen, U., Wesnousky, S.G., Maloney, J., Kent, G., Driscoll, N., 2014. Strike-slip faulting along the Wassuk Range of the northern Walker Lane, Nevada. *Geosphere* 10 (1), 40–48. <http://dx.doi.org/10.1130/GES00912.1>.
- Feng, L., Newman, A.V., 2009. Constraints on continued episodic inflation at Long Valley Caldera, based on seismic and geodetic observations. *J. Geophys. Res.* 114 (B6), B06403. <http://dx.doi.org/10.1029/2008JB006240>.
- Gold, R., dePolo, C., Briggs, R., Crone, A., Gosse, J., 2013. Late Quaternary slip-rate variations along the Warm Springs Valley fault system, Northern Walker Lane, California–Nevada border. *Bull. Seismol. Soc. Am.* 103 (1), 542–558. <http://dx.doi.org/10.1785/0120120020>.
- Gourmelen, N., Amelung, F., 2005. Postseismic mantle relaxation in the central Nevada seismic belt. *Science* 310 (5753), 1473–1476. <http://dx.doi.org/10.1126/science.1119798>.
- Hammond, W.C., Thatcher, W., 2004. Contemporary tectonic deformation of the Basin and Range province, western United States: 10 years of observation with the Global Positioning System. *J. Geophys. Res.* 109, B08403. <http://dx.doi.org/10.1029/2003JB002746>.
- Hammond, W.C., Kreemer, C., Blewitt, G., 2009. Geodetic constraints on contemporary deformation in the northern Walker Lane: 3. Postseismic relaxation in the Central Nevada Seismic Belt. In: Oldow, J.S., Cashman, P. (Eds.), *Late Cenozoic Structure and Evolution of the Great Basin–Sierra Nevada Transition*. In: *Spec. Pap., Geol. Soc. Am.*, vol. 447, pp. 33–54.
- Hammond, W.C., Kreemer, C., Blewitt, G., Plag, H.-P., 2010. Effect of viscoelastic post-seismic relaxation on estimates of interseismic crustal strain accumulation at Yucca Mountain, Nevada. *Geophys. Res. Lett.* 37 (6), L06307. <http://dx.doi.org/10.1029/2010GL042795>.
- Hammond, W.C., Blewitt, G., Kreemer, C., 2011. Block modeling of crustal deformation of the northern Walker Lane and Basin and Range from GPS velocities. *J. Geophys. Res.* 116 (B4), B04402. <http://dx.doi.org/10.1029/2010JB007817>.

- Ichinose, G.A., Anderson, J.G., Smith, K.D., Zeng, Y., 2003. Source parameters of eastern California and western Nevada earthquakes from regional moment tensor inversion. *Bull. Seismol. Soc. Am.* 93 (1), 61–84. <http://dx.doi.org/10.1785/0120020063>.
- Kreemer, C., Blewitt, G., Hammond, W.C., 2009. Geodetic constraints on contemporary deformation in the northern Walker Lane: 2. Velocity and strain rate tensor analysis. In: Oldow, J.S., Cashman, P. (Eds.), *Late Cenozoic Structure and Evolution of the Great Basin–Sierra Nevada Transition*. In: *Spec. Pap., Geol. Soc. Am.*, vol. 447, pp. 17–31.
- Langbein, J., 2003. Deformation of the Long Valley Caldera, California: inferences from measurements from 1988 to 2001. *J. Volcanol. Geotherm. Res.* 127, 247–267. [http://dx.doi.org/10.1016/S0377-0273\(03\)00172-0](http://dx.doi.org/10.1016/S0377-0273(03)00172-0).
- Marshall, G.A., Langbein, J., Stein, R.S., Lisowski, M., Svarc, J., 1997. Inflation of Long Valley Caldera, California, Basin and Range strain, and possible Mono Craters dike opening from 1990–94 GPS surveys. *Geophys. Res. Lett.* 24 (9), 1003–1006.
- McCaffrey, R., 2002. Crustal block rotations and plate coupling. In: Stein, S., Freymueller, J.T. (Eds.), *Plate Boundary Zones*. In: *Geodyn. Ser.*, vol. 30. AGU, Washington, DC, pp. 101–122.
- Meade, B., Hager, B., 2005. Block models of crustal motion in southern California constrained by GPS measurements. *J. Geophys. Res.* 110, B03403. <http://dx.doi.org/10.1029/2004JB003209>.
- Minster, J.B., Jordan, T.H., 1987. Vector constraints on western US deformation from space geodesy, neotectonics, and plate motions. *J. Geophys. Res.* 92 (B6), 4798–4804.
- Nagorsen-Rinck, S., Lee, J., Calvert, A., 2013. Pliocene sinistral slip across the Adobe Hills, eastern California–western Nevada: kinematics of fault slip transfer across the Mina deflection. *Geosphere* 9 (1), 37. <http://dx.doi.org/10.1130/GES00825.S3>.
- Newman, A.V., Dixon, T.H., Ofoegbu, G.I., Dixon, J.E., 2001. Geodetic and seismic constraints on recent activity at Long Valley Caldera, California: evidence for viscoelastic rheology. *J. Volcanol. Geotherm. Res.* 105, 183–206.
- Oldow, J., 2003. Active transtensional boundary zone between the western Great Basin and Sierra Nevada block, western US Cordillera. *Geology* 31 (12), 1033–1036.
- Oldow, J.S., Aiken, C.L.V., Hare, J.L., Ferguson, J.F., Hardyman, R.F., 2001. Active displacement transfer and differential block motion within the central Walker Lane, western Great Basin. *Geology* 29 (1), 19–22.
- Petersen, M.D., Frankel, A.D., Harmsen, S.C., Mueller, C.S., Haller, K.M., Wheeler, R.L., Wesson, R.L., Zeng, Y., Boyd, O.S., Perkins, D.M., Luco, N., Field, E.H., Willis, C.J., Rukstales, K.S., 2008. Documentation for the 2008 update of the United States National Seismic Hazard maps, 61 pp.
- Petronis, M.S., Geissman, J., Oldow, J.S., McIntosh, W.C., 2009. Late Miocene to Pliocene vertical-axis rotation attending development of the Silver Peak–Lone Mountain displacement transfer zone, west-central Nevada. In: Oldow, J.S., Cashman, P.H. (Eds.), *Late Cenozoic Structure and Evolution of the Great Basin–Sierra Nevada Transition*. Geological Society of America, Denver, pp. 215–253.
- Riley, P., Tikoff, B., Hildreth, W., 2012. Transtensional deformation and structural control of contiguous but independent magmatic systems: Mono-Inyo Craters, Mammoth Mountain, and Long Valley Caldera, California. *Geosphere* 8 (4), 740–751. <http://dx.doi.org/10.1130/GES00662.1>.
- Rood, D.H., Burbank, D.W., Finkel, R.C., 2011a. Spatiotemporal patterns of fault slip rates across the Central Sierra Nevada frontal fault zone. *Earth Planet. Sci. Lett.* 301, 457–468. <http://dx.doi.org/10.1016/j.epsl.2010.11.006>.
- Rood, D.H., Burbank, D.W., Herman, S.W., Bogue, S., 2011b. Rates and timing of vertical-axis block rotations across the central Sierra Nevada–Walker Lane tran-
sition in the Bodie Hills, California/Nevada. *Tectonics* 30 (5), TC5013. <http://dx.doi.org/10.1029/2010TC002754>.
- Sarmiento, A.C., Wesnousky, S.G., Bormann, J.M., 2011. Paleoseismic trenches across the Carson and Sierra Nevada range fronts in Antelope Valley, California and Reno, Nevada. *Bull. Seismol. Soc. Am.* 101, 2542–2549. <http://dx.doi.org/10.1785/0120100176>.
- Savage, J.C., 1983. A dislocation model of strain accumulation and release at a subduction zone. *J. Geophys. Res.* 88 (B6), 4984–4996.
- Scherneck, H.-G., 1991. A parameterized solid earth tide model and ocean tide loading effects for global geodetic baseline measurements. *Geophys. J. Int.* 106 (3), 677–694. <http://dx.doi.org/10.1111/j.1365-246X.1991.tb06339.x>.
- Sieh, K., Bursik, M., 1986. Most recent eruption of the Mono Craters, eastern central California. *J. Geophys. Res.* 91 (B12), 12,539–12,571.
- Stewart, J.H., 1988. Tectonics of the Walker Lane Belt, western Great Basin Mesozoic and Cenozoic deformation in a zone of shear. In: Ernst, W.G. (Ed.), *Metamorphism and Crustal Evolution of the Western U.S.*, Ruby Volume VII. Prentice Hall, Englewood Cliffs, NJ, pp. 685–713.
- Surpless, B., 2008. Modern strain localization in the central Walker Lane, western United States: implications for the evolution of intraplate deformation in transtensional settings. *Tectonophysics* 457 (3–4), 239–253. <http://dx.doi.org/10.1016/j.tecto.2008.07.001>.
- Surpless, B., Kroeger, G., 2015. The unusual temporal and spatial slip history of the Wassuk Range normal fault, western Nevada (USA): implications for seismic hazard and Walker Lane deformation. *Geol. Soc. Am. Bull.* 127 (5/6), 737–758. <http://dx.doi.org/10.1130/B31159.1>.
- Taylor, T.R., Dewey, J.F., 2009. Transtensional analyses of fault patterns and strain provinces of the Eastern California shear zone–Walker Lane on the eastern margin of the Sierra Nevada microplate, California and Nevada. *Int. Geol. Rev.* 51 (9–11), 843–872. <http://dx.doi.org/10.1080/00206810903034449>.
- Thatcher, W., Foulger, G.R., Julian, B.R., Svarc, J.L., Quilty, E., Bawden, G.W., 1999. Present-day deformation across the Basin and Range province, western United States. *Science* 283, 1714–1718.
- Unruh, J., Humphrey, J., Barron, A., 2003. Transtensional model for the Sierra Nevada frontal fault system, eastern California. *Geology* 31 (4), 327–330.
- U.S. Geological Survey, California Geological Survey, Nevada Bureau of Mines and Geology, 2006. Quaternary fault and fold database for the United States. Accessed May 2012, from USGS web site: <http://earthquakes.usgs.gov/regional/qfaults/>.
- Wesnousky, S.G., 2005a. Active faulting in the Walker Lane. *Tectonics* 24 (3), TC3009. <http://dx.doi.org/10.1029/2004TC001645>.
- Wesnousky, S.G., 2005b. The San Andreas and Walker Lane fault systems, western North America: transpression, transtension, cumulative slip and the structural evolution of a major transform plate boundary. *J. Struct. Geol.* 27 (8), 1505–1512. <http://dx.doi.org/10.1016/j.jsg.2005.01.015>.
- Wesnousky, S.G., Bormann, J.M., Kreemer, C., Hammond, W.C., Brune, J.N., 2012. Neotectonics, geodesy, and seismic hazard in the Northern Walker Lane of Western North America: thirty kilometers of crustal shear and no strike-slip? *Earth Planet. Sci. Lett.* 329–330 (C), 133–140. <http://dx.doi.org/10.1016/j.epsl.2012.02.018>.
- Wessel, P., Smith, W.H.F., Scharroo, R., Luis, J.F., Wobbe, F.F., 2013. Generic mapping tools: improved version released. *Eos Trans. AGU* 94, 409–410. <http://dx.doi.org/10.1002/2013EO450001>.
- Zumberge, J.F., Heflin, M.B., Jefferson, D.C., Watkins, M.M., Webb, F.H., 1997. Precise point positioning for the efficient and robust analysis of GPS data from large networks. *J. Geophys. Res.* 102 (B3), 5005–5017.